NRC Research Press

ARTICLE

Design of ballasted railway track foundations using numerical modelling. Part I: Development[1]

Md. Abu Sayeed and Mohamed A. Shahin

Abstract: In this paper, a new design method is developed for ballasted railway track foundations that must support high-speed trains and heavy axle loads. The proposed method is intended to prevent the two most common track failures; namely, progressive shear failure of the track subgrade and excessive plastic deformation of the track substructure (i.e., ballast plus subgrade). The method is based on improved empirical models and sophisticated three-dimensional (3D) finite element (FE) numerical analysis. The improved empirical models are used for predicting the cumulative plastic deformation of the track, whereas the stress parameters of the ballast and subgrade layers are obtained from the 3D FE numerical analysis. The outcomes are then synthesized into a set of design charts that form the core of the proposed design method so that it can be readily used by railway geotechnical engineers for routine design practice. The design method can be applied to various practical conditions of train–track–ground systems, including the modulus, thickness, and type of ballast and subgrade. In addition, the traffic parameters that have a significant influence on track performance are also considered in the design method, including the wheel spacing, train speed, and traffic tonnage. The new design method has significant advantages over the existing methods and would provide a major contribution to modern railway track design and code of practice. The applications of the new design method are presented and explained in a companion paper (i.e., Part II: Applications).

Key words: finite elements, numerical modelling, ballasted railway track foundations, subgrade progressive shear failure, track excessive plastic deformation.

Résumé : Dans cet article, une nouvelle méthode de conception est développée pour les fondations de voies ferrées lestéesqui doivent supporter des trains à grande vitesse et des charges d'essieu lourdes. La méthode proposée vise à prévenir deux défaillances de voie les plus courantes, à savoir la rupture progressive de la pente de la voie et la déformation excessive en plastique de la structure de la voie (c.-à-d., ballast et sous-fondation). La méthode est basée sur des modèles empiriques améliorés et une analyse numérique sophistiquée en trois dimensions (3D) des éléments finis (EF). Les modèles empiriques améliorés sont utilisés pour prédire la déformation plastique cumulative de la voie, alors que les paramètres de contrainte des couches de ballast et de sous-fondation sont obtenus à partir d'une analyse numérique EF en 3D. Les résultats sont ensuite synthétisés dans un ensemble de graphiques de conception qui forme le noyau de la méthode de conception proposée afin qu'il puisse être facilement utilisé par les ingénieurs géotechniques ferroviaires pour la pratique de conception de routine. La méthode de conception peut être appliquée à diverses conditions pratiques des systèmes de train–piste–sol, y compris le module, l'épaisseur et le type de ballast et de la sous-fondation. En outre, les paramètres de trafic qui ont une influence significative sur la performance de la voie sont également pris en compte dans la méthode de conception, y compris l'espacement des roues, la vitesse du train et le tonnage du trafic. La nouvelle méthode de conception a des avantages significatifs par rapport aux méthodes existantes et apporterait une contribution majeur dans la conception et le code de pratique moderne d'amure de chemin de fer. Les applications de la nouvelle méthode de conception sont présentées et expliquées dans un document connexe (c.-à-d., Partie II : Applications). [Traduit par la Rédaction]

Mots-clés : éléments finis, modélisation numérique, fondations de voies ferrées lestées, défaillance progressive du cisaillement, déformation plastique excessive de la voie.

Introduction

Recent traffic congestion of highways in many countries around the world has led railways to become the most popular means of public transportation, which has increased the demand for heavier and faster trains. An introduction of heavy axle loads (HALs) and high-speed trains (HSTs) in modern railway traffic creates high stresses in track layers and causes excessive vibrations under train dynamic loading. As a consequence, the risk associated with train operation has increased significantly in the form of train safety, degradation–deformation of track foundations, fatigue failure of rails, and interruption of power supply to trains (Madshus and Kaynia 2000). To avoid such risks and fulfil the demands of modern railway traffic, advanced design methods for ballasted railway track foundations are now warranted and necessary.

Proper design of ballasted railway track foundations entails an accurate estimation of thickness of the granular layer in such a way that it can provide protection against subgrade failure and also limit the excessive track deformation induced by the repetitive moving loads of the train. Granular layer thickness is defined

Received 22 November 2016. Accepted 14 July 2017.

Md.A. Sayeed and M.A. Shahin. Department of Civil Engineering, Curtin University, WA 6845, Australia.

Corresponding author: Mohamed A. Shahin (email: M.Shahin@curtin.edu.au).

[1]This paper is the first of two companion papers published in this issue (Sayeed and Shahin. 2018. Canadian Geotechnical Journal, **55**. dx.doi.org/10.1139/cgj-2016-0634).

Fig. 1. Typical ballasted railway track cross section. [Color online.]

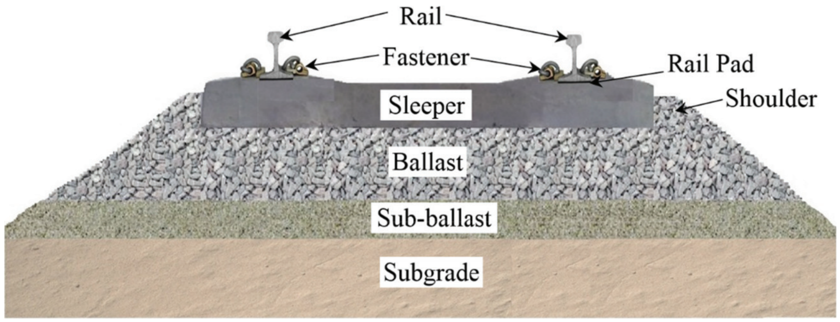

as the combined thickness of ballast and sub-ballast between the sleeper bottom and subgrade surface, as shown in Fig. 1. Conventionally, the design of ballasted railway track foundations is referred to as design of granular layer thickness. Several empirical and simplified theoretical methods have been proposed in the literature to calculate the granular layer thickness, including the American Railway Engineering Association manual (AREA 1996), Canadian modified method suggested by Raymond (1978), Japanese National Railways method developed by Okabe (1961), British Railways method proposed by Heath et al. (1972), and UIC 719 R method offered by the International Union of Railways (UIC 1994). However, most of these methods are based on stress analyses in which all track layers are assumed to be a homogeneous half-space with no allowance for the effect of stiffness of individual track layers. Furthermore, the effect of repeated loading on track settlement has not been included as a design parameter; thus, the application of these oversimplified methods for modern railway track design often provides ballpark estimates and may lead to poor design. The latest and probably the most robust design method currently available in the literature was developed two decades ago by Li and Selig (1998*a*, 1998*b*), which relies on preventing the progressive shear failure and excessive plastic deformation of track subgrade. This method is based on a combined use of a multilayered analytical model called GEOTRACK with extensive cyclic loading laboratory testing. The method has indeed provided some improvement in design of railway track foundations; however, frequent maintenance is still required for tracks designed using the most up-to-date standards that adopt either Li and Selig's (1998*a*, 1998*b*) method or other existing methods. Burrow et al. (2007) reported that the existing design methods may not be appropriate for modern railway traffic. Accordingly, there is an immense need to develop advanced design methods that can overcome and carefully consider the shortcoming of existing methods, leading to more reliable design.

This paper presents the development of a new promising design method for ballasted railway track foundations that overcomes most shortcomings of available design methods. The proposed method is based on modified empirical models and sophisticated three-dimensional (3D) finite element (FE) numerical analysis. The outcomes of the study are employed to develop design charts that form the core of the proposed method so as to facilitate the use of the method by practitioners.

Development of new design method

Over the years, the necessity to overcome shortcomings of most available empirical and analytical approaches for design of railway track foundations has led to the development of numerical methods that have become facilitated by today's high processing capacity of computers. Different numerical modelling approaches have been used in the literature to study the behavior of railway track foundations (e.g., boundary elements method (Andersen and Nielsen 2003), finite elements method (Banimahd et al. 2013; El Kacimi et al. 2013; Hall 2003; Sayeed and Shahin 2015), and 3D finite elements–boundary elements method (Adam et al. 2000; Galvín et al. 2010; O'Brien and Rizos 2005)). Among these approaches, the FE method has been found to be the most useful tool for simulating the critical features of the train–track–ground interaction problem. However, there is still an immense need for a sophisticated 3D FE numerical modelling approach for the development of an advanced design method that can overcome most shortcomings of existing methods; this paper fills in this gap. The main features of the currently available design methods' shortcomings that need to be overcome are discussed below.

To provide a strong, safe, reliable, and efficient pathway for train traffic, the total track deformation should not exceed a prescribed tolerable limit (Shahin 2009). However, the critical factor in relation to deformation of the granular layer is essentially overlooked in all available design methods, despite the fact that ballast can be responsible for up to 40% of total track deformation, as indicated by several researchers (Li et al. 2016; Stewart 1982). To avoid such limitations for an advanced design of track foundations, improved models capable of predicting deformation of both the ballast and subgrade materials should be developed. Furthermore, when a train runs along the track, the ballast and subgrade layers become subjected to complex loading conditions involving principal stress rotation (Brown 1996; Powrie et al. 2007). Accordingly, the train's moving loads (i.e., dynamic cyclic loading with principal stress rotation) may affect the material stiffness and degree of cumulative plastic strain (Inam et al. 2012; Lekarp et al. 2000*a*, 2000*b*). However, a serious shortcoming applied to most or all available design methods is that the subgrade stresses are calculated based on static loading that cannot fully capture the dynamic impact of the moving loads induced by trains.

Existing design methods also consider the effect of train speed by simply utilizing several empirical formulas for estimating the dynamic amplification factor (DAF). However, most available DAF empirical formulas only consider the impact of train speed and loading characteristics, and neglect the characteristics of the track–ground condition. Recent studies carried out by several researchers (e.g., Alves Costa et al. 2015; Sayeed and Shahin 2016*a*) indicated that the DAF is significantly influenced by the subgrade characteristics. Moreover, due to resonance, catastrophic track deflection may occur when the train speed approaches the critical speed (Krylov 1994; Madshus and Kaynia 1999; Yang et al. 2009), which is also significantly influenced by the modulus and thickness of the subgrade medium and train geometry (Alves Costa et al. 2015; Sayeed and Shahin 2016*b*). Unfortunately, there are currently no proper guidelines for considering the critical speed in any available design method. Again, such limitations emphasize the need for developing an advanced design method that can consider the DAF carefully, and can also provide guidelines to determine the critical speed of the train–track–ground system so as to avoid any undesirable failure scenario.

Inspired by the limitations discussed above, a new design method for railway track foundations is proposed in the current paper. To facilitate the use of the new design method by practitioners, a set of design charts that forms the core of the proposed method is developed. The design charts are based on the outcomes of advanced 3D FE analyses and modified empirical models. The affecting design parameters leading to the development of the design method are presented below.

Design criteria

Among several modes of track failures, the two major problems that increase the maintenance costs and reduce the riding quality are the subgrade progressive shear failure and excessive plastic deformation of the track. The focus of the new design method is directed to prevent the progressive shear failure at the subgrade surface and limit the excessive plastic deformation of the track under repeated train dynamic loading. This means that the granular layer thickness should be sufficient so that the stress transferred to the subgrade through the granular media is less than an allowable value suitable for preventing both the subgrade progressive shear failure and excessive track deformation. Preventing the progressive shear failure at the top surface of the subgrade (in the form of plastic flow) can be achieved by limiting the excessive cumulative plastic strain at the subgrade surface. In contrast, limiting the excessive plastic deformation of the track can be achieved by limiting the total plastic deformation accumulated by both the ballast and subgrade sublayers. Accordingly, the design criteria for preventing the progressive shear failure and limiting the excessive track plastic deformation can be characterized by eqs. (1) and (2), as follows:

$$\varepsilon_{p\_s} \le \varepsilon_{(p\_s)a} \tag{1}$$

$$\rho_t = \rho_b + \rho_s \le \rho_{ta} \tag{2}$$

where ε_{p_s} is the cumulative plastic strain at the subgrade surface under repeated loading; $\varepsilon_{(p\_s)a}$ is the allowable plastic strain at the subgrade surface; ρ_t is the total cumulative plastic deformation of the track under repeated train loading; ρ_b and ρ_s are the contributions to track deformation by the ballast and subgrade layers, respectively; and ρ_{ta} is the allowable plastic deformation of the track for the design traffic tonnage.

To fulfil the above design criteria, two strategies can be utilized: (*i*) improving the subgrade stiffness and (*ii*) decreasing the deviatoric stress transmitted to the subgrade by increasing the granular layer thickness. The second strategy is more practical and realistic, and will thus be the focus of this paper. For this strategy to be fulfilled in the proposed design method, a comprehensive study on the strain and deformation characteristics and induced deviatoric stresses of the track substructure is essential, as described below.

Strain and deformation characteristics of track substructure

Subgrade progressive shear failure is most likely to occur in the ballast–subgrade interface, where traffic-induced stresses on the subgrade are very high due to the absence of an granular layer of adequate thickness (Li 1994; Li and Selig 1995). Soil overstressing and repeated cyclic loading can lead to subgrade plastic flow from beneath the track towards the sideway and upward directions, and may cause bearing capacity failure. This phenomenon is known as "cess heave", which is presented in Fig. 2. In addition, the ballasted railway tracks settle as a result of plastic deformations in the ballast layer and underlying subgrade soil caused by the repeated train moving loads. The plastic settlement developed by a single load application may be negligible under general conditions; however, the total cumulative plastic settlement after millions of load cycles may develop to a significant extent where they can severely affect the track performance. Moreover, accumulation of the plastic settlement along and across the track is generally nonuniform, which may lead to undesirable changes in the track geometry.

Fig. 2. Progressive shear failure at subgrade surface. [Color online.]

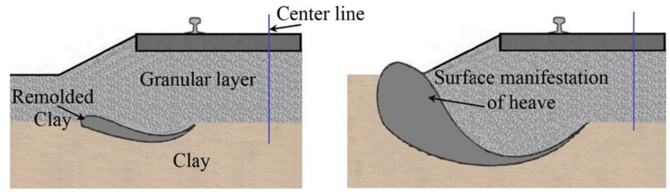

Both subgrade progressive shear failure and track plastic deformation occur due to low stiffness of the ballast and subgrade soil, which are subjected to repeated train moving loads. However, the progressive shear failure is mainly accompanied by an excessive plastic strain at the subgrade surface, whereas the excessive plastic deformation is influenced by the deformable ballast and subgrade layers combined. These two types of track failures can be prevented by providing a sufficient granular layer thickness between the sleeper and subgrade surface. Thereby, an accurate prediction of these two parameters is essential for proper design and maintenance planning of railway tracks. Consequently, as a necessary step in developing the new design method for ballasted railway track foundations, some improved empirical models for predicting the cumulative plastic strain and deformation of ballast and subgrade layers are presented below.

Strain and deformation of ballast

Over the years, a number of studies (e.g., Chrismer and Selig 1993; Indraratna and Salim 2003; Indraratna et al. 2001; Shenton 1975) have investigated the degradation and deformation behavior of ballast materials. These studies resulted in development of several empirical models for determining the accumulated plastic strain and deformation of ballast under repeated loading. However, most of these models were based on strain or deformation incurred after the first load cycle. Also, the applicability of these models is apparently limited to certain ballast types and conditions. Therefore, an improved empirical model that can predict the plastic deformation of ballast with consideration of the major influencing factors (i.e., stress state, physical state, type of ballast, and number of load cycles) is warranted and proposed in this paper. Such a model, as described below, was found to give better predictions of the ballast accumulated plastic deformation.

For the stress state, many researchers (e.g., Alva-Hurtado 1980; Indraratna et al. 2010; Stewart 1982) have indicated that the deviatoric stress is the main stress factor influencing the cumulative plastic strain of ballast under repeated loading rather than the vertical stress or lateral confining stress alone. The plastic strain increases with the increase in deviatoric stress, noting that the deviatoric stress, σ_d, is the difference between the major and minor principal stresses (i.e., $\sigma_d = \sigma_1 - \sigma_3$). As shear stress of the ballast is basically half the deviatoric stress, the deviatoric stress can be considered to represent the physical condition of the shear stress. Therefore, the value of confining pressure, σ_3, is a secondary factor.

The physical state of ballast can be defined by its void ratio, gradation, moisture content, and ballast structure. Many test results (e.g., Indraratna and Salim 2003; Raymond and Diyaljee 1979) have reported significant effects of the ballast physical state on the cumulative plastic deformation. For example, the ballast materials having a small initial void ratio are stronger in shear and generate a smaller deformation than their counterparts having a higher initial void ratio. To consider the influence of the ballast physical state, it is neither useful nor common to include the ballast parameters, such as the void ratio, gradation, moisture content, and ballast structure, directly into an empirical model. However, the influence of these parameters can rather be indirectly repre-

Table 1. Material parameters for various types of ballast.

Ballast type	x	y	z
Basalt	4.82	1.42	0.49
Granite	1.27	2.41	0.48
Dolomite	4.23	1.15	0.32

sented by the strength of ballast under monotonic triaxial loading tests. This is because the ballast strength depends on the void ratio, gradation, moisture content, and ballast structure. In addition, the monotonic triaxial tests can be routinely performed in any soil mechanics laboratory.

In this paper, an empirical model is proposed for predicting the ballast cumulative plastic strain for three different types of ballast; namely, basalt, granite, and dolomite. It should be noted that the model is a modified version of a previous model developed by the second author (i.e., Shahin 2009), and is based on data obtained from a series of large-scale triaxial, isotropically consolidated, drained cyclic compression tests available in the literature (e.g., Alva-Hurtado 1980; Lackenby et al. 2007; Raymond and Williams 1978). The redeveloped model is given as follows:

$$\varepsilon_{\mathrm{p\_b}} = \frac{x(\alpha)^y[1 + \ln(N_{\mathrm{b}})]^z}{100} \tag{3}$$

where $\varepsilon_{\mathrm{p\_b}}$ is the cumulative plastic strain of the ballast; $\alpha = \sigma_{\mathrm{d\_b}}/\sigma_{\mathrm{s\_b}}$ ($\sigma_{\mathrm{d\_b}}$ is the applied cyclic deviatoric stress and $\sigma_{\mathrm{s\_b}}$ is the compressive strength of the ballast under 50 kPa confining pressure, which can be obtained from a monotonic triaxial test); N_{b} is the number of load applications on the ballast; and x, y and z are material parameters that depend on the ballast type as given in Table 1. These parameters are determined from a regression analysis carried out on the data obtained from the cyclic triaxial loading tests conducted on the ballast. Figure 3 shows the model calibration and predictions for different ballast types, including basalt (Fig. 3*a*), granite (Fig. 3*b*), and dolomite (Fig. 3*c*). It can be seen that the influence of the stress state, physical state, and type of ballast on the cumulative plastic strain are well reflected in the model predictions.

For a particular ballasted railway track, the cumulative plastic strain of the ballast, $\varepsilon_{\mathrm{p\_b}}$, after N_{b} load cycles can be determined by knowing the value of the deviatoric stress applied to the ballast layer, $\sigma_{\mathrm{d\_b}}$. Then, the accumulation of plastic deformation can be determined by summing up the deformations of all subdivided layers, using the following equation:

$$\rho_{\mathrm{b}} = \sum \varepsilon_{(\mathrm{p\_b})i} H_{\mathrm{b}i} \tag{4}$$

where ρ_{b} is the plastic deformation of the ballast layer, $\varepsilon_{(\mathrm{p\_b})i}$ is the plastic strain at the centre of each ballast sublayer, and $H_{\mathrm{b}i}$ is the thickness of each sublayer of the ballast. It is recommended to determine the deviatoric stress from 3D FE numerical modelling, as will be described later. It should be noted that when a train passes along the track, the ballast particles are subjected to a complex loading that involves principal stress rotation. However, the empirical model developed above is based on data obtained from traditional cyclic triaxial tests in which the major principal stresses are not rotated. Therefore, it would be useful in the future to examine deformation behavior of the ballast under real loading conditions by considering cyclic loading with principal stress rotation, and incorporating this effect into the empirical model.

Fig. 3. Calibration of developed empirical model for ballast plastic strain with experimental results: (*a*) basalt; (*b*) granite; (*c*) dolomite.

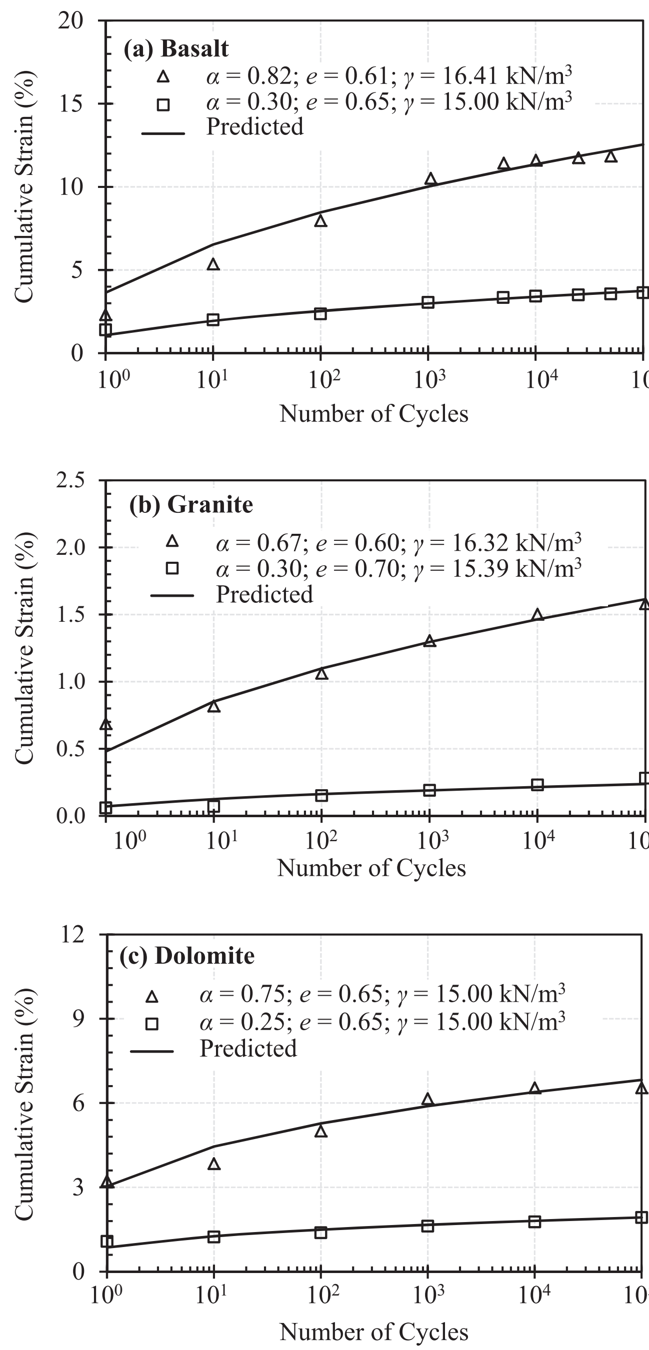

Strain and deformation of subgrade

In the past, a large number of cyclic loading triaxial or direct shear tests were conducted on either unsaturated or saturated soil samples under undrained or drained conditions, to investigate the plastic deformation of fine-grained soils for repeated loading. Based on experimental data collected from these tests, various models were proposed for estimating the cumulative plastic strain of fine-grained soils. Among these models, the most advanced ones that are currently used to predict the cumulative plastic strain and cumulative plastic deformation of track fine-grained subgrade soils are those developed by Li (1994) and Li and Selig (1996), as follows:

Table 2. Material parameters for subgrade soil types CH, CL, MH, and ML (modified after data from Li and Selig 1998*a*).

Material parameter	High-plasticity clay (CH)	Low-plasticity clay (CL)	High-plasticity silt (MH)	Low-plasticity silt (ML)
a	1.20	1.10	0.84	0.64
b	0.18	0.16	0.13	0.10
m	2.40	2.00	2.00	1.70

$$\varepsilon_{\mathrm{p\_s}} = \frac{a}{100}\left(\frac{\sigma_{\mathrm{d\_s}}}{\sigma_{\mathrm{s\_s}}}\right)^m N_\mathrm{s}^b \tag{5}$$

$$\rho_\mathrm{s} = \sum \varepsilon_{(\mathrm{p\_s})i} H_{\mathrm{s}i} \tag{6}$$

where $\varepsilon_{\mathrm{p\_s}}$ is the cumulative plastic strain of the track subgrade soil; $\sigma_{\mathrm{d\_s}}$ is the deviatoric stress applied to the subgrade; $\sigma_{\mathrm{s\_s}}$ is the unconfined compressive strength of the subgrade soil; N_s is the number of load repetitions applied to the subgrade layer; *a*, *b*, and *m* are material parameters given in Table 2; ρ_s is the cumulative plastic deformation of the track subgrade; $\varepsilon_{(\mathrm{p\_s})i}$ is the plastic strain at the center of each subdivided subgrade layer calculated using eq. (5); and $H_{\mathrm{s}i}$ is the thickness of each sublayer of the subgrade.

In eq. (5), the effect of the soil stress state (i.e., deviatoric stress) on the relationship between the cumulative plastic strain of the subgrade and number of load applications is considered directly. In addition, the influence of the soil physical state (e.g., water content, dry density, and soil structure) on the subgrade performance is represented indirectly by the static soil strength, $\sigma_{\mathrm{s\_s}}$, which is linked directly to the soil physical state and its structure. The influence of the soil type is implied by the material parameters (*a*, *b*, and *m*). Thus, the effect of all major influencing factors affecting the cumulative plastic strain of the subgrade soil (i.e., number of repeated stress applications, soil stress state, soil type, and soil physical state) are reflected in the developed prediction model. Therefore, the empirical model adopted in eq. (5) is used in the current work for development of the design charts that will be described later.

Deviatoric stress characteristics of track substructure

A key element in the development of the ballasted railway track design method is the accurate calculation of distribution of deviatoric stress caused by true train moving loads in the granular and subgrade layers under various train–track–ground conditions, including moduli and thicknesses of the ballast and subgrade. To this end, this section is devoted to the analyses of the deviatoric stress generation within the track foundation using an advanced 3D FE numerical modelling subjected to true train moving loads, as explained below.

The 3D FE numerical model developed in this paper was previously established by the authors (Sayeed and Shahin 2015, 2016*b*) and validated against data of field measurements obtained from Cunha and Correia (2012) and Kaynia et al. (2000). The 3D FE numerical model is used herein to investigate the dynamic response of the train–track–ground system subjected to train moving loads, for the deviatoric stress analyses, which is shown in Fig. 4. The dimensions of the 3D FE model are 80 m, 36 m, and 7.5 m in the longitudinal, horizontal, and vertical directions, respectively. The rail is modelled using a one-dimensional (1D) I-beam section running across the length of the modelled track. A UIC 60 section is assumed for the rail, which is fixed to the sleepers by rail pads characterized by an elastic link (spring-like) element of stiffness equal to 100 MN/m. All other track components (i.e., sleeper, ballast, interface, and subgrade) are modelled using 3D solid elements, and it is assumed that the granular layer is characterized only by the ballast layer. For the model geometry, a total of 133 sleepers are placed along the rail at 0.6 m interval. The ballast layer is modelled using elastoplastic Mohr–Coulomb (MC) materials, whereas the other track materials are considered to be linear elastic (LE) materials. The material properties of the track model are given in Table 3, and the range of variables considered are given in Table 4.

The element size of the FE model is generally estimated based on the smallest wavelength that allows the high-frequency motion to be simulated correctly. Accordingly, the sizes of the 3D FE in the current study are taken to be 0.167 m × 0.137 m × 0.2 m, 0.2 m × 0.2 m × 0.2 m, and 0.6 m × 0.6 m × 0.6 m for the sleepers, ballast, and subgrade, respectively. Overall, the FE mesh consists of 285 000 elements. The model vertical boundaries are connected to viscous dampers to absorb the incident *S*- and *P*-waves to represent infinite boundary conditions, as suggested by many researchers (e.g., Kouroussis et al. 2011; Lysmer and Kuhlemeyer 1969). The nodes at the bottom boundary are set to be fixed in every direction to simulate bedrock. The material damping of the FE model is characterized by the mass and stiffness proportional coefficients, typically referred to as the Rayleigh damping, which is commonly used in the dynamic analyses.

In the current analyses, the standard X-2000 passenger train is considered to be moving along the modelled track, and the approach of simulating the moving loads is taken to be the same as that described in previous papers published by the authors (Sayeed and Shahin 2016*a*, 2016*b*). The train geometry and standard axle loads of the X-2000 high speed train (HST) are summarized in Table 5, including (for each car number) the distance between axles (L_a), distance between two bogies (L_b), carriage length (L_c), front wheel load (P_F), and rear wheel load (P_R). Figure 5 shows a schematic diagram of the X-2000 HST and its components.

Distribution of deviatoric stress along the rail

The characteristics of the deviatoric stress distribution along the rail at the ballast surface (i.e., zero depth below the sleeper bottom) and at the subgrade surface (i.e., below the granular layer) are shown in Fig. 6. It can be seen from Fig. 6*a* that the maximum deviatoric stresses induced at the ballast surface beneath the sleepers are almost constant after the passage of the X-2000 HST along the track. However, the deviatoric stresses at the same depth of the ballast below the crib are less than those beneath the sleeper. In contrast, it can be seen from Fig. 6*b* that the deviatoric stress distribution along the rail at the subgrade surface is almost invariant. However, for the purpose of design of railway track foundations, the deviatoric stress distribution along the depth of the ballast and subgrade layers can be selected below the sleeper rather than the crib, which is the zone of the maximum deviatoric stress.

Distribution of deviatoric stress along the sleeper

Figure 7 shows the deviatoric stress distribution along the sleeper at four different depths of ballast (Fig. 7*a*) and three different depths of subgrade (Fig. 7*b*) from the sleeper bottom. It can be seen from Fig. 7*a* that the deviatoric stress of the ballast at various depths bellow the sleeper is minimum at the track centre and maximum at the sleeper end. However, variation of the deviatoric stress distribution along the sleeper reduces with depth below the sleeper. Similarly, it can be seen from Fig. 7*b* that the deviatoric stress at a depth equal to 0.45 m below the sleeper bottom (i.e., at the subgrade surface) is maximum at the end of the sleeper. However, with the increase in depth below the sleeper bottom, the distribution of the deviatoric stress in the subgrade along the sleeper becomes almost uniform. Therefore, for the purpose of design of railway track foundations, it can be considered that the maximum deviatoric stress occurs below the sleeper end.

Fig. 4. Developed 3D FE numerical model of ballasted railway track. [Color online.]

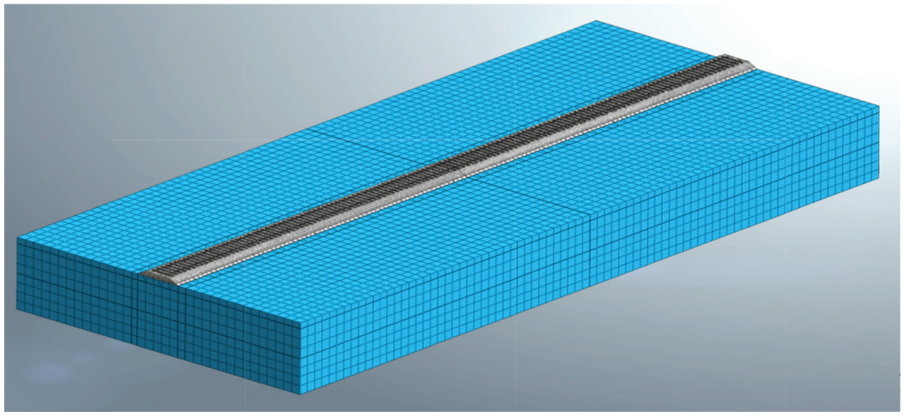

Table 3. Material properties used in the FE numerical modelling.

Track component	Material property	Value
Rail	Dynamic modulus of elasticity, E (MPa)	210 000
	Poisson's ratio, ν	0.30
	Moment of inertia, I (m^4)	3.04×10^{-5}
Sleeper	Dynamic modulus of elasticity, E (MPa)	30 000
	Poisson's ratio, ν	0.20
	Unit weight, γ (kN/m^3)	20.2
	Length, l (m)	2.50
	Width, w (m)	0.27
	Thickness (m)	0.20
Ballast	Dynamic modulus of elasticity, E (MPa)	270
	Poissons ratio, ν	0.30
	Unit weight, γ (kN/m^3)	17.3
	Cohesion, c (kPa)	0.00
	Friction angle, ϕ (°)	50.0
	Thickness, H (m)	0.45
	Shear wave velocity, C_s (m/s)	243
	Damping ratio, ξ	0.03
Subgrade soil	Dynamic modulus of elasticity, E (MPa)	60.0
	Poissons ratio, ν	0.35
	Unit weight, γ (kN/m^3)	18.8
	Thickness, H (m)	7.50
	Shear wave velocity, C_s (m/s)	108
	Raleigh wave velocity, C_R (m/s)	101
	Damping ratio, ξ	0.03

Table 4. Range of variable track properties used in the deviatoric stress analysis.

Parameter	Lower bound	Nominal	Upper bound
Ballast modulus, E_b (MPa)	135	270	540
Subgrade modulus, E_s (MPa)	15	60	120
Ballast thickness, H_b (m)	0.15	0.45	1.35
Subgrade thickness, H_s (m)	3.75	7.50	10.00

Table 5. Geometry and axle loads of the X-2000 HST (modified after data from Takemiya 2003).

	Spacing (m)			Standard wheel load (kN)	
Car number, n	L_a	L_b	L_c	P_F	P_R
1	2.9	14.5	22.2	81.0	61.3
2	2.9	17.7	24.4	61.3	61.3
3	2.9	17.7	24.4	61.3	61.3
4	2.9	17.7	24.4	61.3	61.3
5	2.9	9.5	17.2	90.0	90.0

Fig. 5. Geometry of X-2000 HST used for FE numerical modelling. [Color online.]

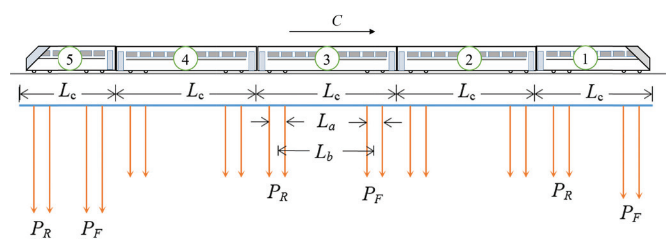

Effect of ballast and subgrade stiffness on deviatoric stress

Figure 8 presents the distribution of the maximum deviatoric stress with depth in the granular layer for various substructure conditions, including the ballast modulus (Fig. 8*a*) and subgrade modulus (Fig. 8*b*). It can be seen from Fig. 8*a* that the deviatoric stress diminishes with depth of the granular layer, for all values of the ballast modulus. However, the stress dissipation is not the same; it is higher for stiffer ballast. It can also be seen that the deviatoric stress developed at the ballast surface is greater for a higher ballast modulus. In contrast, it can be seen from Fig. 8*b* that the deviatoric stress induced at the ballast surface increases with the decrease of subgrade stiffness, indicating a significant stress generation in the ballast layer supported by the soft subgrade, which might increase the ballast particle breakage and can lead to ballast fouling. It can also be seen that the stress distribution efficiency for the ballast layer is higher when the subgrade is softer.

Figure 9 presents the distribution of deviatoric stress with depth in the subgrade layer, for various substructure conditions, including the ballast modulus (Fig. 9*a*) and subgrade modulus (Fig. 9*b*). It can be seen from Fig. 9*a* that an increase in the ballast modulus decreases the deviatoric stress, at all depths within the subgrade layer. On the contrary, it can be seen from Fig. 9*b* that an increase in the subgrade modulus significantly increases the deviatoric stress at the subgrade surface. However, the difference in the deviatoric stress (due to different subgrade stiffness) at each depth below the sleeper bottom decreases with depth.

Effect of granular layer thickness on deviatoric stress

The impact of granular layer thickness, H_b, on the distribution of deviatoric stress with depth for the subgrade is investigated by considering a range of ballast thicknesses from 0.15 to 1.35 m. The impact of the granular layer thickness on the deviatoric stress distribution within the subgrade is studied for two type of subgrade materials, including the soft subgrade (Fig. 10*a*) and stiff

Fig. 6. Deviatoric stress along rail at surface for (*a*) ballast and (*b*) subgrade. [Color online.]

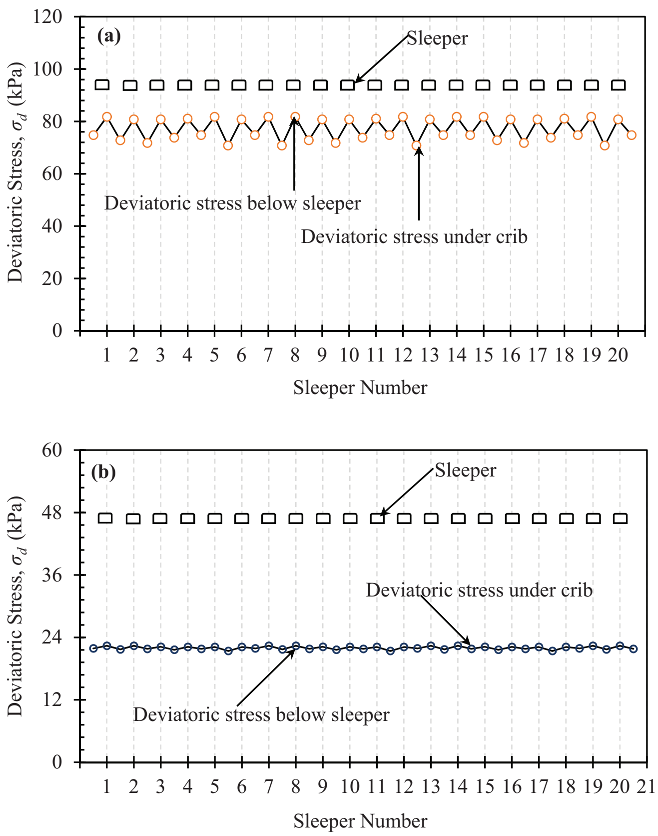

subgrade (Fig. 10*b*). The soft subgrade is characterized herein by a dynamic subgrade modulus equal to 15 MPa, while the stiff subgrade is represented by a dynamic modulus of 120 MPa. It can be seen from Fig. 10 that the increase in the granular layer thickness leads to a significant reduction in the deviatoric stress at the subgrade surface. It is also evident from Fig. 10*a* that a significant difference in the deviatoric stress occurs at each depth below the bottom of sleeper due to the corresponding difference in the granular layer thickness, and this difference reduces with distance below the sleeper. However, in contrast to the soft subgrade condition, Fig. 10*b* shows that the difference in the deviatoric stress due to the change in granular layer thickness below the bottom of sleeper is almost negligible in the case of stiff subgrade for all depths. In essence, the increase in the granular layer thickness reduces the distribution of the deviatoric stress within the subgrade in two ways. Firstly, when the granular layer thickness increases, the distance of the subgrade surface below the bottom of sleeper is automatically increased. Consequently, the deviatoric stress at the subgrade surface is automatically decreased by virtue of the depth spreading effect. Secondly, with the increase of the granular layer thickness (i.e., stiffer layer), the stress spreading effect also increases, which leads to a reduction in the deviatoric stress at all depths in the subgrade. However, the second effect weakens when the difference in the stiffness of the granular and subgrade layers becomes smaller. Therefore, when the subgrade soil modulus is closer to that of the ballast, the effect of the granular layer thickness on the distribution of the deviatoric stress in the subgrade becomes insignificant.

Effect of subgrade layer thickness on deviatoric stress

The impact of the subgrade layer thickness on the distribution of deviatoric stress within the subgrade is investigated by considering three different subgrade thicknesses (i.e., H_s = 3.5, 7.0, and 10 m), overlying a hard rock, and the results are shown in Fig. 11. It can be seen that the difference in the deviatoric stress at each depth of the subgrade is negligible, except at the interface of the subgrade with the hard rock. As the influence of subgrade thickness on the distribution of deviatoric stress in the subgrade is insignificant, the subgrade thickness is assumed to be fixed at 7.0 m in the deviatoric analysis performed for development of the design charts used in the proposed design method.

Traffic parameters

The proposed design method for ballasted railway track foundations emphasizes the influence of the following traffic parameters on track performance: wheel spacing, train speed, and traffic tonnage. For the purpose of presenting the effects of the abovementioned traffic parameters on track performance, the 3D FE model of the X-2000 HST (Fig. 4) and its track properties (Table 3) described earlier are used.

The impact of train wheel spacing on the track dynamic response, which has been incorporated in the track design procedures described in the companion paper (Sayeed and Shahin 2018; hereafter referred to as “Part II: Applications”), is investigated and presented in this section. For this purpose, six different values of wheel spacing (i.e., L_a = 1.6, 1.8, 2.2, 2.6, 3.0, and 3.4 m) are considered for the X-2000 HST. This range of wheel spacing is selected carefully to reflect the practical range expected in major trains including freight and high-speed passenger trains (Colaço et al. 2016; Jeffs and Tew 1991). The influence of wheel spacing on track deflection is shown in Fig. 12. It can be seen from Fig. 12*a* that track deflection increases with the decrease in wheel spacing, as expected. To quantify the impact of wheel spacing in the proposed design method, a relationship between wheel spacing and the wheel spacing factor (WSF) is developed and presented in Fig. 12*b*. The WSF is defined as the ratio of track deflection at a particular wheel spacing to track deflection at the standard wheel spacing for the X-2000 HST. It can be seen from Fig. 12*b* that the effect of wheel spacing can be reduced significantly by increasing the spacing between train wheels.

Available design methods usually consider the effect of train speed and loading characteristics by simply utilizing several empirical formulas that neglect the characteristics of subgrade conditions. However, it was found by Sayeed and Shahin (2016*a*, 2016*b*) that track response is significantly influenced by the subgrade stiffness and thickness. Therefore, for development of the new design method, the effects of train speed on track performance are investigated under various subgrade conditions and have been later incorporated in the track design procedures described in the companion paper (i.e., Part II: Applications). Five different values of subgrade modulus (i.e., E_s = 15, 30, 60, 90, and 120 MPa) and four different track subgrade thicknesses (i.e., H_s = 5, 7.5, 10, and ∞ m) overlying a hard bedrock are utilized. The results are presented in Fig. 13 in terms of the relationship between train speed and DAF. The DAF is defined as the ratio of the maximum dynamic sleeper deflection at a particular train speed to the maximum quasi-static sleeper deflection (i.e., sleeper deflection at a train speed of 5 m/s). Figure 13 shows the evolution of the DAF for the sleeper downward deflection versus train speed, for different subgrade stiffnesses and subgrade thicknesses. It can be seen that, for all values of E_s and H_s, the DAF increases with the increase in train speed until it reaches a peak value corresponding to the critical speed, after which it decreases with further increase in train speed. Figure 13 also indicates that the DAF decreases with the increase in both the subgrade stiffness and thickness. In contrast, the magnitude of the critical speed increases with the increase in subgrade stiffness, while it decreases with the increase in subgrade thickness. The practical implication of this finding is that the localized ground improvement of the soft subgrade can be very beneficial in decreasing the DAF and increasing the critical speed of trains.

Fig. 7. Deviatoric stress along sleeper at different depths with (*a*) ballast and (*b*) subgrade.

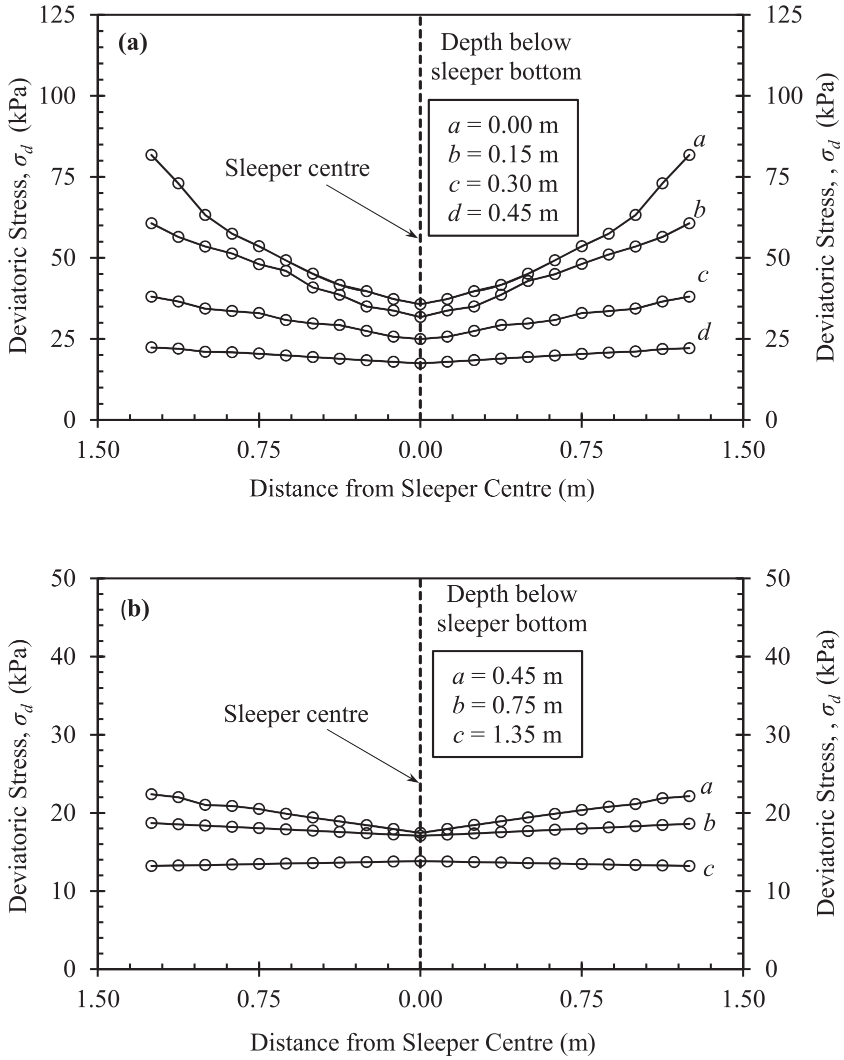

The design traffic tonnage is the total possible amount of load in million gross tonnes (MGT) that needs to be carried along the track without causing track failure. This value should be selected based on the maintenance costs and traffic speed restriction considerations. The traffic parameters mentioned earlier are used to calculate three design variables for the design traffic tonnage: (*i*) dynamic wheel load, P_d; (*ii*) total equivalent number of load applications in the ballast layer, N_b; and (*iii*) total equivalent number of load applications in the subgrade layer, N_s. The design dynamic wheel load corresponding to the maximum static wheel load, train speed, and wheel spacing of the moving train can be determined as follows:

$$P_d = P_s(\mathrm{WSF})(\mathrm{DAF}) \tag{7}$$

where P_d is the design dynamic wheel load; P_s is the maximum static wheel load of the train, assumed to run along the track; WSF is the wheel spacing factor (Fig. 12*b*) based on the impact of the wheel spacing of any train with respect to the standard wheel spacing of the X-2000 HST; and DAF is the dynamic amplification factor based on the train speed and subgrade condition (Fig. 13).

It is generally assumed that when a train runs along the track, two axles under the same bogie produce one load cycle in the ballast layer whereas four axles under two adjacent bogies (carriages) produce a single load cycle in the subgrade layer (Li et al. 2016). Therefore, for any particular wheel load, P_{si}, the number of load cycles in the ballast, N_{bi}, and in the subgrade, N_{si}, can be determined as follows:

$$N_{bi} = \frac{T_i}{4P_{si}} \tag{8}$$

$$N_{si} = \frac{T_i}{8P_{si}} \tag{9}$$

where T_i is the total traffic tonnage of the wheel load, P_{si}, in the same unit as P_{si}. To consider the influence of different amplitudes of wheel loading on subgrade performance, the number of load cycles in the subgrade, N_{si}, for wheel loading, P_{si}, can be converted to an equivalent number of load cycles, N_{si}^0, of the maximum static wheel load, P_s, as follows (Li and Selig 1996):

$$N_{si}^0 = N_{si}\left(\frac{P_{si}}{P_s}\right)^{m/b} \tag{10}$$

where m and b are material parameters dependent on the subgrade soil type (Table 2). Similarly, the number of load cycles in the ballast, N_{bi}, for wheel load, P_{si}, can be converted to an equiva-

Fig. 8. Distribution of deviatoric stress with depth for ballast layer at various (*a*) ballast moduli and (*b*) subgrade moduli.

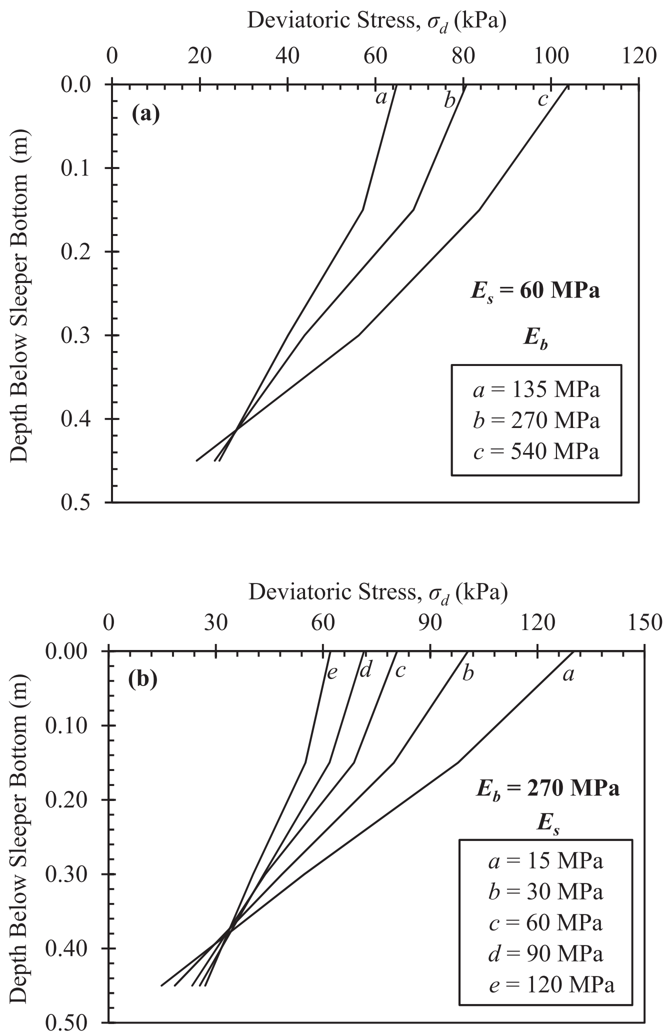

Fig. 9. Distribution of deviatoric stress with depth for subgrade layer at various (*a*) ballast moduli and (*b*) subgrade moduli.

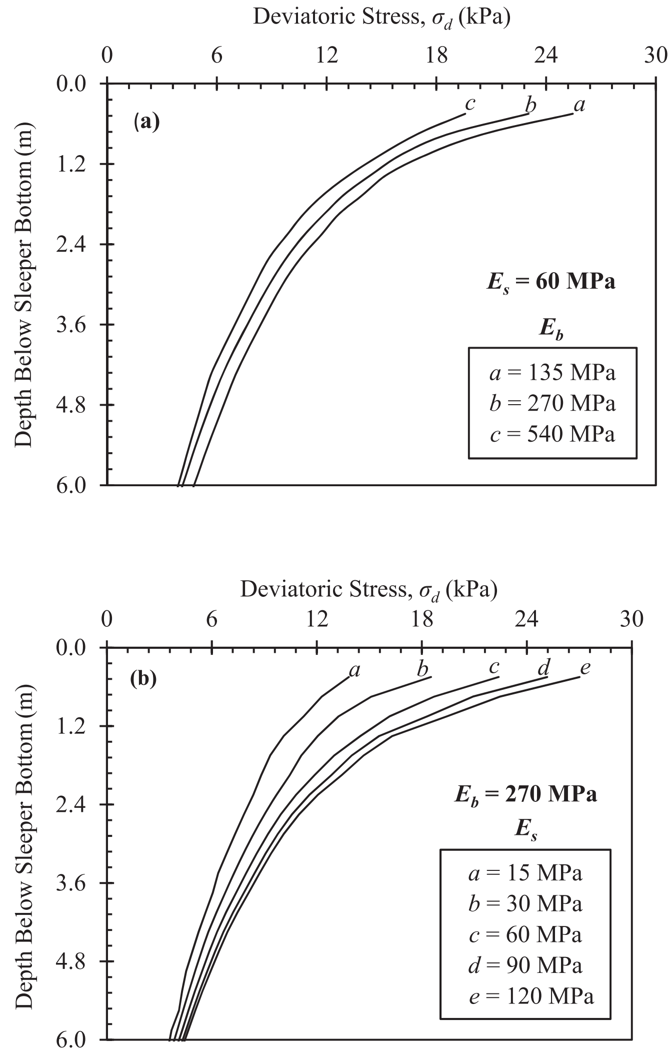

lent load cycle, N^0_{bi}, corresponding to the maximum static wheel load, P_s, as follows:

$$N^0_{bi} = N_{bi}\left(\frac{P_{si}}{P_s}\right)^{y/z} \tag{11}$$

where y and z are material parameters dependent on the ballast type (given in Table 1). Accordingly, the total number of equivalent load applications in both the ballast layer (N_b) and subgrade layer (N_s) corresponding to the maximum static wheel load, P_s, can be calculated as follows:

$$N_b = N^0_{bi} + N^1_{bi} + N^2_{bi} + N^3_{bi} + \ldots + N^n_{bi} \tag{12}$$

$$N_s = N^0_{si} + N^1_{si} + N^2_{si} + N^3_{si} + \ldots + N^n_{si} \tag{13}$$

Design principles and options

As mentioned earlier, the two criteria that need to be achieved for design of railway track foundations are (*i*) limiting the cumulative plastic strain at the subgrade surface and (*ii*) limiting the total plastic deformation of the track layers to a value below a tolerable level, as represented earlier by eqs. (1) and (2). The procedures that need to be followed to achieve an appropriate design using the above two design criteria are explained in this section. For convenience, the distinction between the ballast and subballast is ignored by simply presenting the ballast layer as the granular layer.

For particular loading conditions and characteristics of the granular and subgrade layers, the design of ballasted railway track is relevant to selecting an adequate granular layer thickness so that the deviatoric stress experienced by the substructure layers is adequately low. Thus, the possibility of occurrence of progressive shear failure at the subgrade surface and excessive plastic deformation of the track can be prevented. Based on this principle, the first phase of developing the railway track design charts involves determining the deviatoric stresses in the ballast and subgrade, for a range of granular layer and subgrade conditions. Calculation of the deviatoric stress is performed using the advanced 3D FE modelling subjected to quasi-static (i.e., at speed = 5 m/s) train moving loads of the X-2000 HST, for a total of 105 cases with various combinations of ballast and subgrade characteristics. The parameters assumed include the ballast modulus (i.e., E_b = 135, 270, and 540 MPa), subgrade soil modulus (i.e., E_s = 15, 30, 60, 90, and 120 MPa), and granular layer thickness (i.e., H_b = 0.15, 0.30, 0.45, 0.60, 0.75, 1.05, and 1.35 m). The other track parameters are fixed at their nominal values given earlier in Table 3. The ranges selected above and those in Table 3 for all material parameters have been selected carefully to reflect the practical range expected in major railway tracks (Li 1994; Li and Selig 1994). It should be noted that although the deviatoric stresses for development of

Fig. 10. Effect of granular layer thickness on distribution of deviatoric stress with depth for (*a*) soft subgrade and (*b*) stiff subgrade.

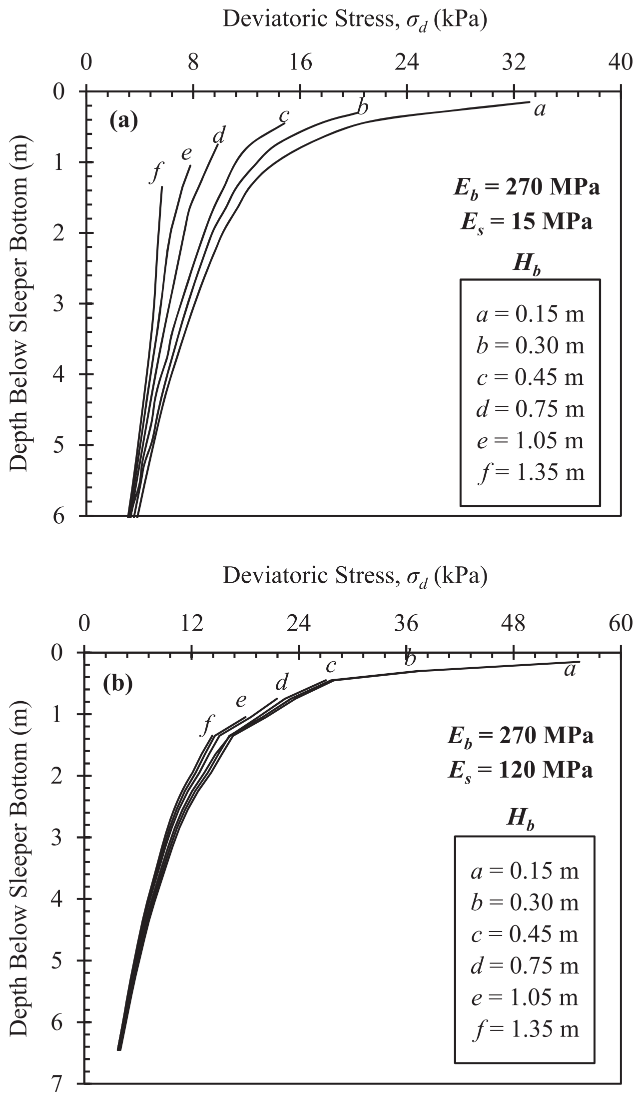

Fig. 11. Distribution of deviatoric stress with depth in subgrade layer for different subgrade thicknesses.

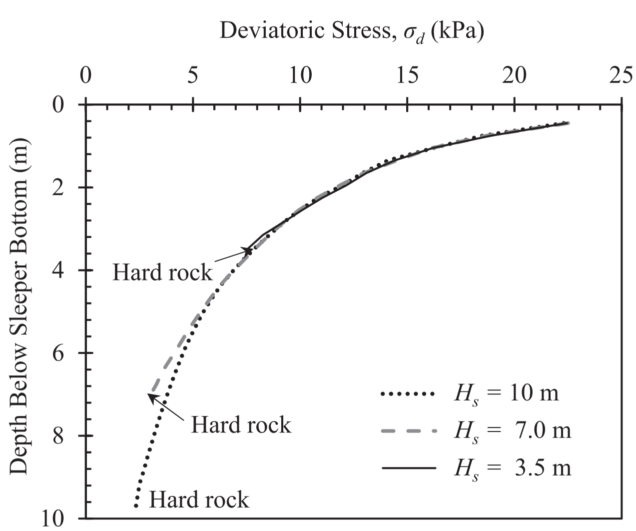

Fig. 12. Relationship between (*a*) track deflection versus wheel spacing and (*b*) wheel spacing factor versus wheel spacing.

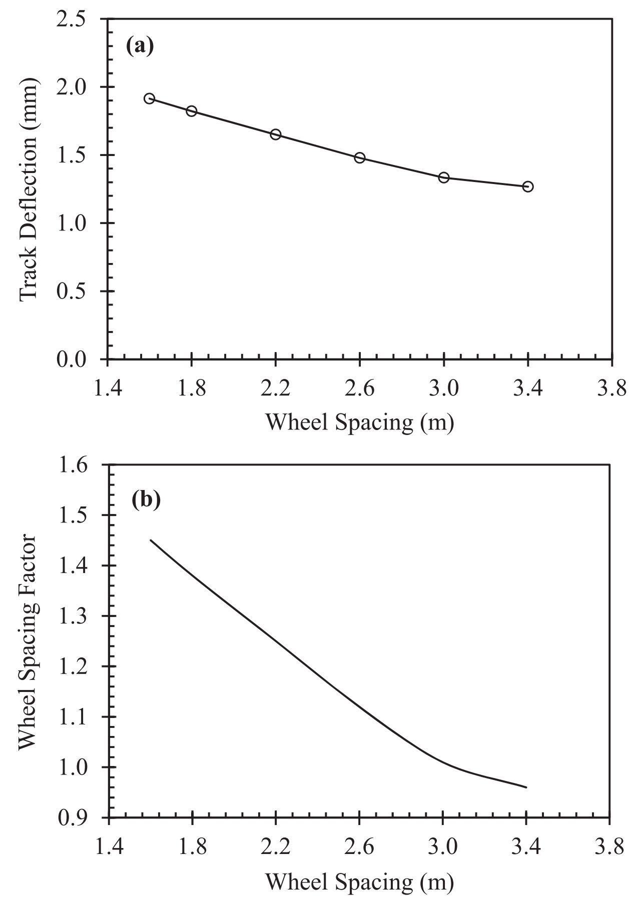

the design charts are calculated based on a specific train geometry (i.e., X-2000 HST wheel spacing) and train speed (i.e., 5 m/s), the impact of any other train geometry or train speed are incorporated later in the design procedure so that the design charts can be used universally for any train loading conditions.

Design for preventing progressive shear failure

The design criterion for preventing progressive subgrade failure is to limit the cumulative plastic strain at the subgrade surface below an allowable value. As indicated earlier in eq. (5), the principle of keeping the cumulative plastic strain below a certain tolerable level means limiting the deviatoric stress. The deviatoric stress at the subgrade surface for different substructure conditions is readily calculated using the earlier developed 3D FE modelling. As calculation of the deviatoric stress assumes linear elastic–plastic ballast and linear elastic subgrade, the ratio of deviatoric stress to design dynamic wheel load is set to be constant for a given track–ground condition. For illustration, the time history responses for the deviatoric stress and strain at the subgrade surface under three different amplitudes of loading for the X-2000 HST (i.e., 100%, 150%, and 200% of the standard X-2000 HST) are depicted in Fig. 14. It can be seen that both the deviatoric stress (Fig. 14*a*) and deviatoric strain (Fig. 14*b*) under the passing wheel loads increase with the increase of loading amplitudes. The obtained results indicate that the maximum deviatoric stress and strain increase linearly with the loading amplitudes, which allowed the development of the following dimensionless strain influence factor:

Fig. 13. Evolution of dynamic amplification factor versus train speed under various subgrade conditions: (a) H_s = 5.0 m; (b) H_s = 7.5 m; (c) H_s = 10.0 m; (d) H_s = ∞.

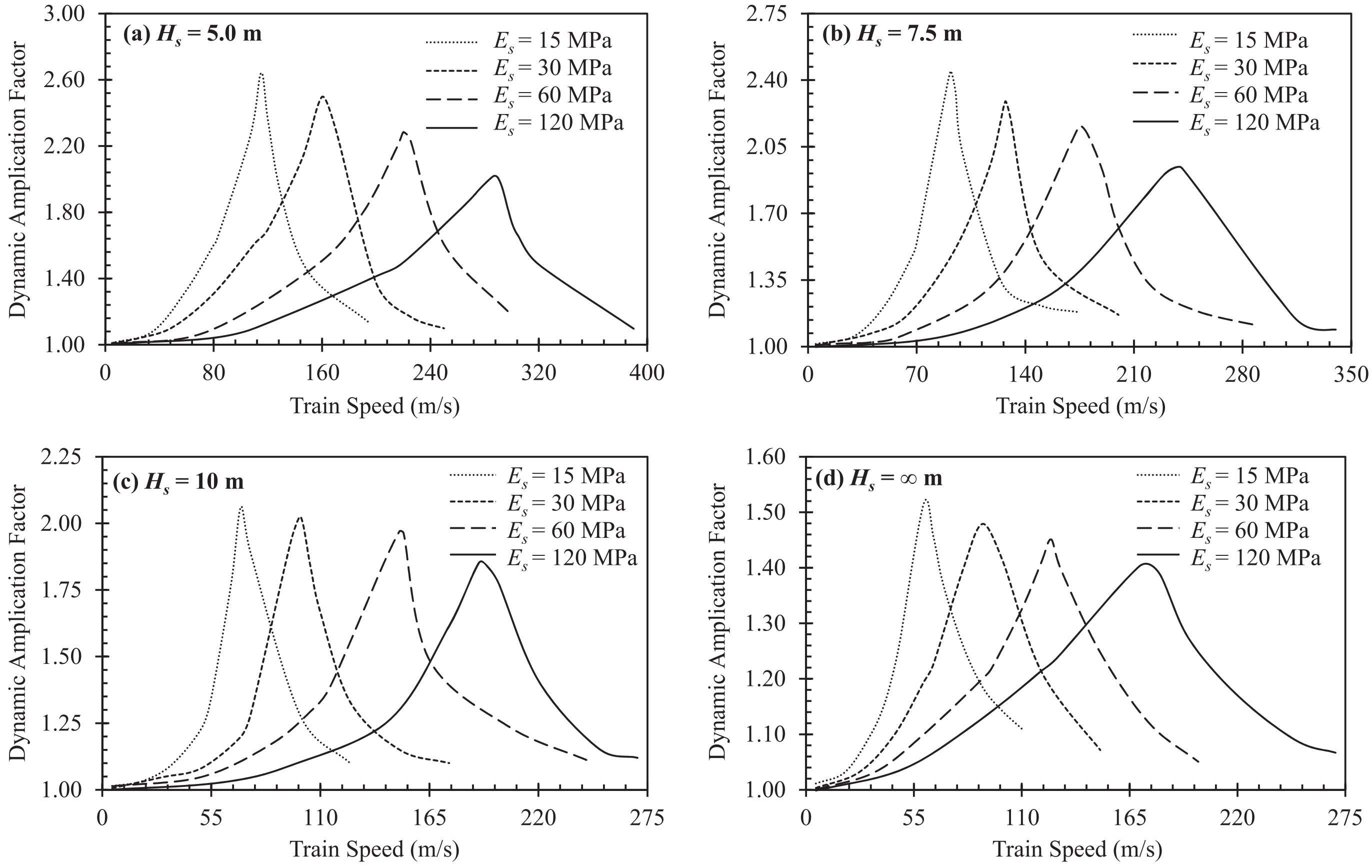

Fig. 14. Influence of loading amplitudes on time history for (a) deviatoric stress and (b) deviatoric strain. [Color online.]

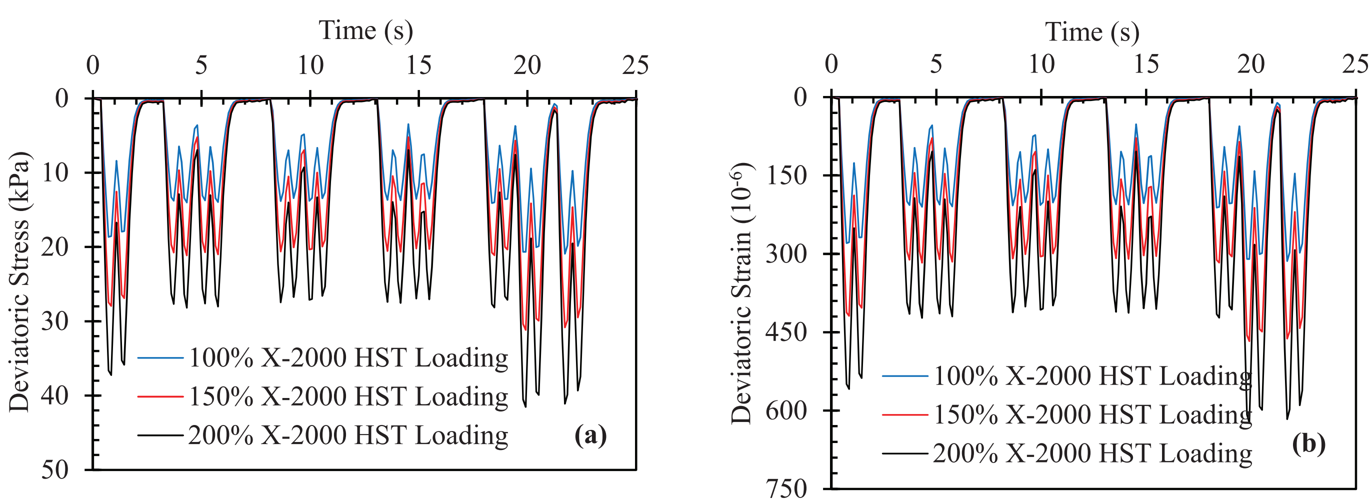

$$I_\varepsilon = \frac{\sigma_d A}{P_d} \tag{14}$$

where I_ε is the strain influence factor; σ_d is the deviatoric stress; P_d is the design dynamic wheel load, which can be calculated using eq. (7); and A is an area coefficient to make the strain influence factor dimensionless (A unit value of 1 m² is assumed for the ease of calculation).

The strain influence factor generated at the subgrade surface, I_{ε_s}, from the FE analyses for various substructure conditions can now be readily synthesized into simple design charts, which are built to calculate the granular layer thickness needed to prevent the progressive shear failure. An example of these design charts is shown in Fig. 15, in which each curve corresponds to a particular ballast and subgrade moduli. The complete set of design charts encompassing other design parameters are given in Appendix A of the companion paper (i.e., Part II: Applications), which are employed to calculate the granular layer thicknesses for four track sites and the results have been compared with field measurements.

Fig. 15. Example of design chart for calculation of granular layer thickness to prevent progressive shear failure.

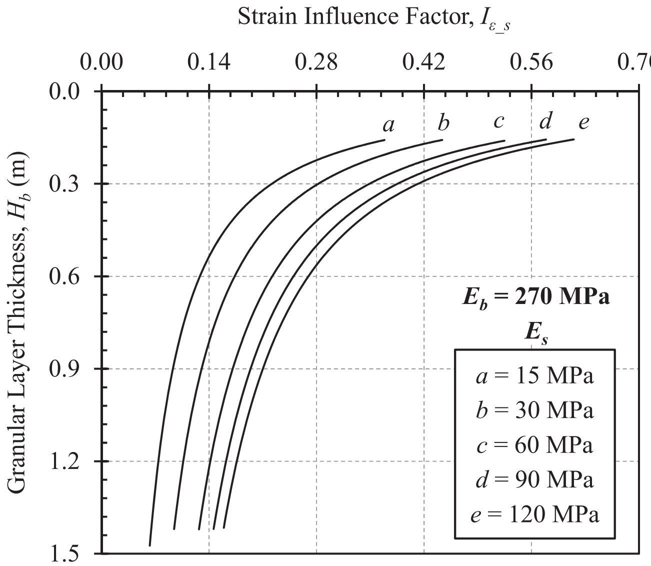

Fig. 16. Development of curve "*a*" of Fig. 15 from Fig. 10*a* for the substructure with E_b = 270 MPa and E_s = 15 MPa: (*a*) strain influence factor versus depth below sleeper bottom and (*b*) strain influence factor versus granular layer thickness.

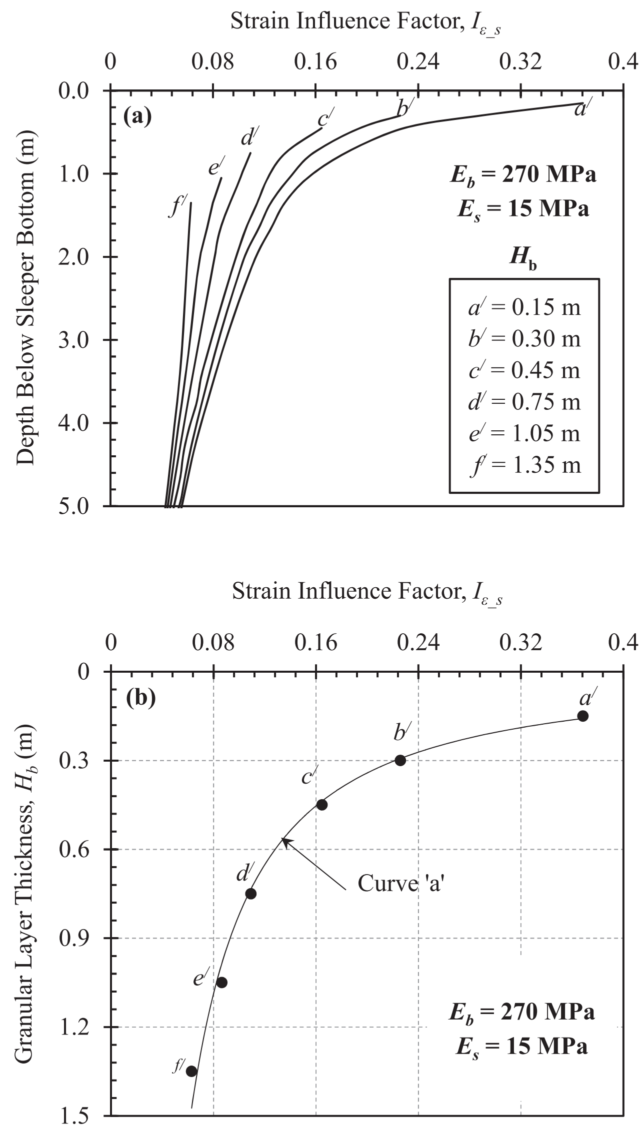

The development process of the relationship between the granular layer thickness, H_b, and strain influence factor at the subgrade surface, I_{ε_s}, is illustrated in Fig. 16. As the process for a certain combination of E_b and E_s is identical, only the establishment of curve "*a*" of Fig. 15 for the substructure with a specific modulus of ballast and subgrade (i.e., E_b = 270 MPa and E_s = 15 MPa) is shown in Fig. 16. For this purpose, Fig. 16*a* is first regenerated from Fig. 10*a* by simply replacing the deviatoric stress with the strain influence factor using eq. (14). It can be seen from Fig. 16*a* that the strain influence factor at the subgrade surface, I_{ε_s}, decreases with the increase of granular layer thickness, H_b. To develop the design charts, the resulting strain influence factors at the subgrade surface, I_{ε_s}, are plotted against H_b for a particular set of granular layer and subgrade moduli, as shown in Fig. 16*b*.

To apply the proposed design method using the design charts (e.g., Fig. 15), the minimum required thickness of the granular layer can be determined for an acceptable value of the subgrade surface strain influence factor, $I_{(\varepsilon\_s)a}$. Therefore, the value of $I_{(\varepsilon\_s)a}$ needs to be determined using eq. (15) below, obtained by rearranging eq. (14) and substituting $I_{(\varepsilon\_s)a}$ and $\sigma_{(d\_s)a}$ for I_ε and σ_d, respectively, as follows:

$$I_{(\varepsilon\_s)a} = \frac{\sigma_{(d\_s)a} A}{P_d} \tag{15}$$

where $I_{(\varepsilon\_s)a}$ is the allowable strain influence factor at the subgrade surface; $\sigma_{(d\_s)a}$ is the allowable deviatoric stress at the subgrade surface; P_d is the design dynamic wheel load, which can be calculated using eq. (7); and A is the area coefficient (= 1 m²). In addition, the allowable deviatoric stress at the subgrade surface, $\sigma_{(d\_s)a}$, can be calculated using eq. (16) below, which is derived by rearranging eq. (5) and substituting $\sigma_{(d\_s)a}$ and $\varepsilon_{(p\_s)a}$ for σ_{d_s} and ε_{p_s}, respectively, as follows:

$$\sigma_{(d\_s)a} = \left(\frac{\varepsilon_{(p\_s)a}}{aN_s^b}\right)^{\frac{1}{m}} \sigma_{s\_s} \times 100 \tag{16}$$

where $\varepsilon_{(p\_s)a}$ is the allowable cumulative plastic strain at the subgrade surface needed for preventing the progressive shear failure; σ_{s_s} is the soil compressive strength; a, b, and m are the material parameters pertinent to the subgrade soil type (Table 2); N_s is the total equivalent number of repeated applications of the design load on the subgrade.

Design for preventing excessive plastic deformation

The key principle of preventing excessive plastic deformation in the track is limiting the track deformation to a value below a tolerable level. Therefore, the total cumulative plastic deformation due to repeated loading in the substructure layers, ρ_t, (i.e., granular ballast layer thickness, H_b, and subgrade layer thickness, H_s) needs to be determined by summing the integration of the cumulative plastic strain of the ballast (i.e., eq. (3)) and subgrade (i.e., eq. (5)) layers, as follows:

$$\rho_t = \rho_b + \rho_s = \int_0^{H_b} \frac{x[1 + \ln(N_b)]^z}{100} \left(\frac{\sigma_{d\_b}}{\sigma_{s\_b}}\right)^y dh + \int_0^{H_s} \frac{aN_s^b}{100} \left(\frac{\sigma_{d\_s}}{\sigma_{s\_s}}\right)^m dh \tag{17}$$

Fig. 17. Example of distribution of strain influence factor with depth in ballast layer.

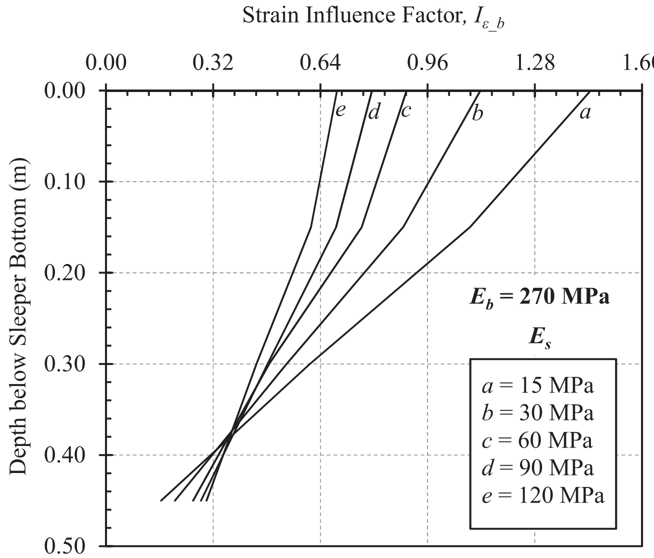

Rearranging eq. (17) yields

$$\text{(18)} \qquad \rho_t = \frac{x[1 + \ln(N_b)]^z}{100}\left(\frac{P_d}{A\sigma_{s\_b}}\right)^y \int_0^{H_b} \left(\frac{A\sigma_{d\_b}}{P_d}\right)^y dh + \frac{aLN_s^b}{100}\left(\frac{P_d}{A\sigma_{s\_s}}\right)^m \int_0^{H_s} \left(\frac{A\sigma_{d\_s}}{P_d}\right)^m \frac{dh}{L}$$

Using the definition of the strain influence factor (i.e., eq. 14), eq. (18) can be expressed as follows:

$$\text{(19)} \qquad \rho_t = \frac{x[1 + \ln(N_b)]^z}{100}\left(\frac{P_d}{A\sigma_{s\_b}}\right)^y \int_0^{H_b} (I_{\varepsilon\_b})^y\, dh + \frac{aLN_s^b}{100}\left(\frac{P_d}{A\sigma_{s\_s}}\right)^m \int_0^{H_s} (I_{\varepsilon\_s})^m \frac{dh}{L}$$

As indicated by eq. (19), deformation of the track substructure layers is a function of the strain influence factor, which is a function of the deviatoric stress in the ballast and subgrade. Therefore, the deviatoric stress distribution with depth within the ballast and subgrade layers for different substructure conditions is readily calculated using the earlier developed 3D FE modelling subjected to the moving loads of the X-2000 HST. Afterwards, the results are presented in terms of the distribution of strain influence factor with depth using eq. (14). Figure 17 shows an example of the distribution of the dimensionless strain influence factor, I_{ε_b}, with depth in the ballast layer for a particular ballast modulus (i.e., E_b = 270 MPa) and thickness (i.e., H_b = 0.45 m) for different values of the subgrade modulus. It should be noted that Fig. 17 is simply a reproduction of Fig. 8*b*, in which the axis of the deviatoric stress is replaced by the strain influence factor using eq. (14). Similarly, the distribution of I_{ε_b} with depth in the ballast layer for different substructure conditions (i.e., different moduli and thicknesses of ballast and subgrade) are presented in Appendix B of the companion paper (Part II: Applications).

The deformation generated in the ballast layer, ρ_b, for the associated track substructure conditions can be determined using the results of Appendix B (e.g., Fig. 17) in the companion paper and the following equation, which is the first part of eq. (19):

$$\text{(20)} \qquad \rho_b = \frac{x[1 + \ln(N_b)]^z}{100}\left(\frac{P_d}{A\sigma_{s\_b}}\right)^y \int_0^{H_b} (I_{\varepsilon\_b})^y\, dh$$

The integration in eq. (20) can be solved by dividing the granular ballast layer into sublayers of thicknesses = 0.1–0.15 m, then the integration is obtained by summing the multiplication of the strain influence factor at the middle of each sublayer by the corresponding sublayer thickness.

To develop the design charts for preventing the excessive plastic deformation of track, the second part of eq. (19), which quantifies the cumulative plastic deformation of the subgrade layer, can be rearranged as follows:

$$\text{(21)} \qquad \rho_s = \frac{aLN_s^b}{100}\left(\frac{P_d}{A\sigma_{s\_s}}\right)^m \int_0^{H_s} (I_{\varepsilon\_s})^m \frac{dh}{L} = \left[\frac{aLN_s^b}{100}\left(\frac{P_d}{A\sigma_{s\_s}}\right)^m\right] I_{\rho\_s}$$

thus

$$\text{(22)} \qquad I_{\rho\_s} = \int_0^{H_s} (I_{\varepsilon\_s})^m \frac{dh}{L}$$

where I_{ρ_s} is a dimensionless deformation influence factor. It should be noted that both the area coefficient (A) and length coefficient (L) are used in eqs. (18)–(22) for the purpose of nondimensionalizing the strain and deformation influence factors. Similar to the area coefficient, a unit value is assumed for the length coefficient (i.e., L = 1 m) for the ease of calculation.

As indicated in eq. (22), the subgrade deformation influence factor, I_{ρ_s}, is a function of the distribution of the strain influence factor, I_{ε_s}, with the depth of subgrade, type of subgrade, and thickness of subgrade, H_s. It should be noted that the distribution of I_{ε_s} with depth in the subgrade is governed by different combinations of E_b, E_s, and H_b. Accordingly, the values of I_{ρ_s} are calculated using eq. (22) and the distribution of strain influence factor, I_{ε_s}, with depth of the subgrade for different combinations of E_b, E_s, H_b, and H_s, and the parameter m depends on the subgrade soil type. To produce the design charts, the values of the resulting I_{ρ_s} are plotted against H_b for particular granular ballast and subgrade layer conditions. Figure 18 shows two samples of the design charts that can be used to calculate the granular layer thickness needed to prevent the excessive plastic deformation. Each chart corresponds to one soil type and one modulus combination of the granular and subgrade layers, and each curve corresponds to one deformable subgrade layer thickness. Following the same process mentioned above, a total of 60 design charts have been developed and given in Appendix C of the companion paper (i.e., Part II: Applications).

To apply the proposed design method for estimating the granular layer thickness, the first step is to determine the cumulative plastic deformation in the initially assumed thickness of the granular ballast layer, ρ_b, as explained above. Then, the allowable subgrade deformation influence factor, $I_{(\rho\_s)a}$, needs to be calculated using eq. (23) below, obtained by rearranging eq. (21) and substituting ($\rho_t - \rho_b$) for ρ_s and ρ_{ta} for ρ_t, as follows:

$$\text{(23)} \qquad I_{(\rho\_s)a} = \frac{\rho_{ta} - \rho_b}{\dfrac{aLN_s^b}{100}\left(\dfrac{P_d}{A\sigma_{s\_s}}\right)^m}$$

where ρ_{ta} is the allowable track deformation; ρ_b is the contribution of track deformation of the ballast layer; N_s is the total equivalent number of load repetitions in the subgrade for the design traffic tonnage; P_d is the design dynamic wheel load; σ_{s_s} is the

Fig. 18. Design charts to calculate granular layer thickness for preventing excessive plastic deformation: (*a*) E_s = 15 MPa; (*b*) E_s = 30 MPa.

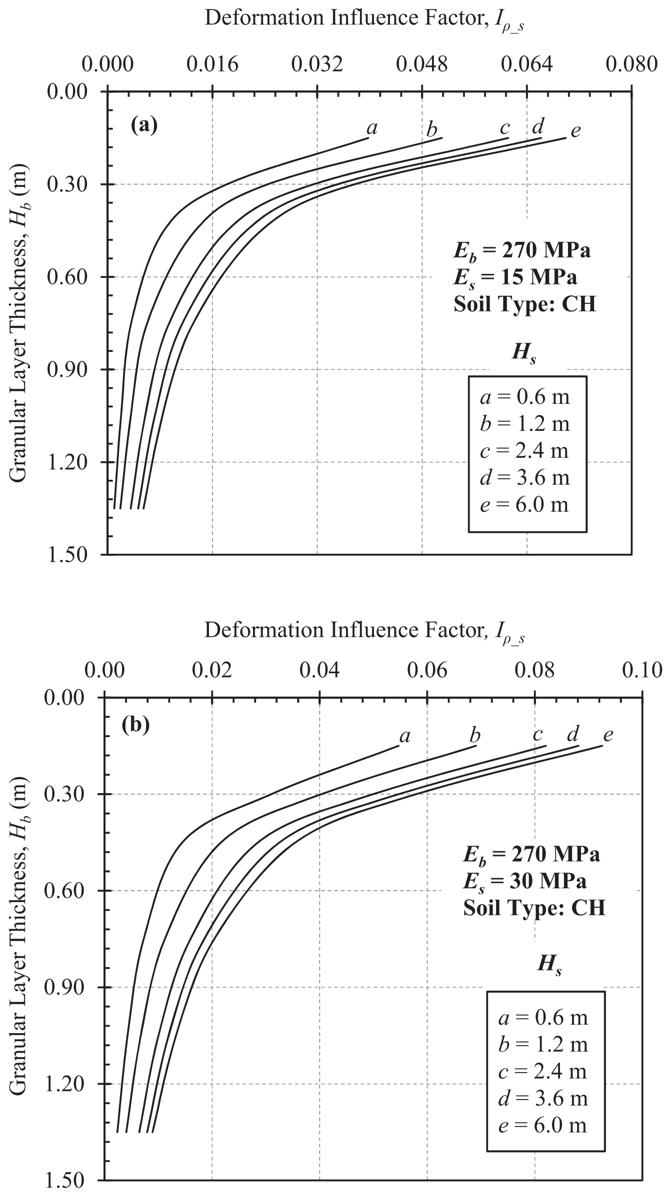

unconfined compressive strength of subgrade soil; *a*, *b*, and *m* are material parameters dependent on the subgrade soil type (see Table 2); *A* is the area coefficient (= 1 m²); and *L* is the length coefficient (= 1 m).

After determining $I_{(\rho\_s)a}$, the required granular layer thickness, H_b, can be obtained using the relevant design chart (e.g., Fig. 18*a*) from Appendix C given in the companion paper (i.e., Part II: Applications), based on the specific data of ballast modulus, E_b, subgrade modulus, E_s, subgrade layer thickness, H_s, and subgrade soil type. If the thickness obtained from the design chart is not equal to the initially assumed granular layer thickness, H_b, the steps of calculating ρ_b for an obtained thickness, $I_{(\rho\_s)a}$, and H_b should be repeated until the granular layer thickness considered in the calculation of ρ_b converges with the thickness obtained from the design charts.

Full details in relation to the procedures for using the design method for calculating H_b utilizing the developed design charts and applications of the new design method to real track situations are described in detail in the companion paper (i.e., Part II: Applications).

Summary and conclusions

In this paper, a new practical design method for ballasted railway track foundations was developed to overcome most shortcomings of the existing design methods. The proposed method is meant to prevent two common track failures; namely, subgrade progressive shear failure and excessive track deformation. The proposed design method was developed based on improved empirical models and sophisticated 3D FE numerical analysis. The improved empirical models were used for predicting the cumulative plastic deformation of the track, whereas the stress behavior of ballast and subgrade under applications of train repeated loadings were determined from the 3D FE numerical modelling. In the improved empirical models, the effects of number of load applications, stress state, physical state, and material type were considered. The impact of stress state was explicitly represented by the induced deviator stress while the material physical state was indirectly specified by its monotonic strength obtained from the conventional triaxial compression tests. The material type was considered through certain material parameters involved. In the 3D FE modelling, the dynamic response of railway tracks under a variety of train–track–ground conditions was investigated and quantified. The practical implications of the obtained results were critically analysed and discussed to facilitate the development of the proposed design method.

The results obtained from the study were synthesized into a set of design charts that form the core of the proposed design method so that the method can be readily used by railway geotechnical engineers for routine design practice. All governing parameters that significantly affect the selection of the granular layer thickness for preventing track failure were carefully considered in the proposed design method. The verification and application of the proposed design method are presented in a companion paper (i.e., Part II: Applications) and the results have been found to be in excellent agreement with field observations. It is believed that the proposed design method is expected to provide a significant contribution to the current railway track code of practice.

References

Adam, M., Pflanz, G., and Schmid, G. 2000. Two- and three-dimensional modelling of half-space and train-track embankment under dynamic loading. Soil Dynamics and Earthquake Engineering, **19**(8): 559–573. doi:10.1016/S0267-7261(00)00068-3.

Alva-Hurtado, J.E.D. 1980. A methodology to predict the elastic and inelastic behavior of railroad ballast. Dissertation, Department of Civil Engineering. University of Massachusetts, Amherst, Mass.

Alves Costa, P., Colaço, A., Calçada, R., and Cardoso, A.S. 2015. Critical speed of railway tracks. Detailed and simplified approaches. Transportation Geotechnics, **2**: 30–46. doi:10.1016/j.trgeo.2014.09.003.

Andersen, L., and Nielsen, S.R. 2003. Boundary element analysis of the steady-state response of an elastic half-space to a moving force on its surface. Engineering Analysis with Boundary Elements, **27**(1): 23–38. doi:10.1016/S0955-7997(02)00096-6.

AREA. 1996. Manual for railway engineering. Vol. 1. American Railway Engineering Association (AREA), Washington, D.C.

Banimahd, M., Woodward, P., Kennedy, J., and Medero, G. 2013. Three-dimensional modelling of high speed ballasted railway tracks. Proceedings of the Institution of Civil Engineers - Transport, **166**(2): 113–123. doi:10.1680/tran.9.00048.

Brown, S.F. 1996. Soil mechanics in pavement engineering. Géotechnique, **46**(3): 383–426. doi:10.1680/geot.1996.46.3.383.

Burrow, M.P.N., Bowness, D., and Ghataora, G.S. 2007. A comparison of railway track foundation design methods. Proceedings of the Institution of Mechanical Engineers, Part F: Journal of Rail and Rapid Transit, **221**(1): 1–12. doi:10.1243/09544097jrrt58.

Chrismer, S., and Selig, E.T. 1993. Computer model for ballast maintenance planning. *In* Proceedings of the 5th International Heavy Haul Railway Conference. pp. 223–227.

Colaço, A., Costa, P.A., and Connolly, D.P. 2016. The influence of train properties on railway ground vibrations. Structure and Infrastructure Engineering, **12**(5): 517–534. doi:10.1080/15732479.2015.1025291.

Cunha, J., and Correia, A.G. 2012. Evaluation of a linear elastic 3D FEM to simulate rail track response under a high-speed train. *In* Proceedings of ICTG - Advances in Transportation Geotechnics II. *Edited by* Miura et al. Taylor & Francis, Balkema, London. pp. 196–201.

El Kacimi, A., Woodward, P.K., Laghrouche, O., and Medero, G. 2013. Time domain 3D finite element modelling of train-induced vibration at high speed. Computers & Structures, **118**: 66–73. doi:10.1016/j.compstruc.2012.07.011.

Galvín, P., Romero, A., and Domínguez, J. 2010. Fully three-dimensional analysis of high-speed train-track-soil-structure dynamic interaction. Journal of Sound and Vibration, **329**(24): 5147–5163. doi:10.1016/j.jsv.2010.06.016.

Hall, L. 2003. Simulations and analyses of train-induced ground vibrations in finite element models. Soil Dynamics and Earthquake Engineering, **23**(5): 403–413. doi:10.1016/S0267-7261(02)00209-9.

Heath, D.L., Shenton, M.J., Sparrow, R.W., and Waters, J.M. 1972. Design of conventional rail track foundations. Proceedings of the Institution of Civil Engineers, **51**: 251–267. doi:10.1680/iicep.1972.5952.

Inam, A., Ishikawa, T., and Miura, S. 2012. Effect of principal stress axis rotation on cyclic plastic deformation characteristics of unsaturated base course material. Soils and Foundations, **52**(3): 465–480. doi:10.1016/j.sandf.2012.05.006.

Indraratna, B., and Salim, W. 2003. Deformation and degradation mechanics of recycled ballast stabilised with geosynthetics. Soils and Foundations, **43**(4): 35–46. doi:10.3208/sandf.43.4_35.

Indraratna, B., Salim, W., Ionescu, D., and Christie, D. 2001. Stress-strain and degradation behaviour of railway ballast under static and dynamic loading, based on large-scale triaxial testing. *In* Proceedings of the 15th International Conference on Soil Mechanics and Geotechnical Engineering, Istanbul. pp. 2093–2096.

Indraratna, B., Thakur, P.K., and Vinod, J.S. 2010. Experimental and numerical study of railway ballast behavior under cyclic loading. International Journal of Geomechanics, **10**(4): 136–144. doi:10.1061/(ASCE)GM.1943-5622.0000055.

Jeffs, T., and Tew, G.P. 1991. A review of track design procedures. Vol. 2: Sleepers and ballast. BHP Research - Melbourne Laboratories.

Kaynia, A.M., Madshus, C., and Zackrisson, P. 2000. Ground vibration from high-speed trains: prediction and countermeasure. Journal of Geotechnical and Geoenvironmental Engineering, **126**(6): 531–537. doi:10.1061/(ASCE)1090-0241(2000)126:6(531).

Kouroussis, G., Verlinden, O., and Conti, C. 2011. Finite-dynamic model for infinite media: corrected solution of viscous boundary efficiency. Journal of Engineering Mechanics, **137**(7): 509–511. doi:10.1061/(ASCE)EM.1943-7889.0000250.

Krylov, V.V. 1994. On the theory of railway-induced ground vibrations. Journal de Physique, **4**(C5): 769–772. doi:10.1051/jp4:19945167.

Lackenby, J., Christie, D., Indraratna, B., and McDowell, G. 2007. Effect of confining pressure on ballast degradation and deformation under cyclic triaxial loading. Géotechnique, **57**(6): 527–536. doi:10.1680/geot.2007.57.6.527.

Lekarp, F., Isacsson, U., and Dawson, A. 2000*a*. State of the art. I: Resilient response of unbound aggregates. Journal of Transportation Engineering, **126**(1): 66–75. doi:10.1061/(ASCE)0733-947X(2000)126:1(66).

Lekarp, F., Isacsson, U., and Dawson, A.R. 2000*b*. State of the art. II: Permanent strain response of unbound aggregates. Journal of Transportation Engineering, **126**(1): 76–83. doi:10.1061/(ASCE)0733-947X(2000)126:1(76).

Li, D. 1994. Railway track granular layer thickness design based on subgrade performance under repeated loading. Dissertation, Department of Civil and Environmental Engineering, University of Massachusetts, Amherst, Mass.

Li, D., and Selig, E.T. 1994. Resilient modulus for fine-grained subgrade soils. Journal of Geotechnical Engineering, **120**(6): 939–957. doi:10.1061/(ASCE)0733-9410(1994)120:6(939).

Li, D., and Selig, E.T. 1995. Evaluation of railway subgrade problems. Transportation Research Record, **1489**: 17–25.

Li, D., and Selig, E.T. 1996. Cumulative plastic deformation for fine-grained subgrade soils. Journal of Geotechnical Engineering, **122**(12): 1006–1013. doi:10.1061/(ASCE)0733-9410(1996)122:12(1006).

Li, D., and Selig, E.T. 1998*a*. Method for railroad track foundation design. I: Development. Journal of Geotechnical and Geoenvironmental Engineering, **124**(4): 316. doi:10.1061/(ASCE)1090-0241(1998)124:4(316).

Li, D., and Selig, E.T. 1998*b*. Method for railroad track foundation design. II: Applications. Journal of Geotechnical and Geoenvironmental Engineering, **124**(4): 323. doi:10.1061/(ASCE)1090-0241(1998)124:4(323).

Li, D., Hyslip, J., Sussmann, T., and Chrismer, S. 2016. Railway Geotechnics. CRC Press, Tailor & Francis Group, Boca Raton, Fla.

Lysmer, J., and Kuhlemeyer, R.L. 1969. Finite dynamic model for infinite media. Journal of the Engineering Mechanics Division, ASCE, **95**(EM4): 859–877.

Madshus, C., and Kaynia, A.M. 1999. Dynamic ground interaction; a critical issue for high speed train lines on soft soil. *In* Geotechnical engineering for transportation infrastructure. *Edited by* Barends et al. Balkema, Amsterdam, the Netherlands. pp. 1–8.

Madshus, C., and Kaynia, A.M. 2000. High-speed railway lines on soft ground: dynamic behaviour at critical train speed. Journal of Sound and Vibration, **231**(3): 689–701. doi:10.1006/jsvi.1999.2647.

O'Brien, J., and Rizos, D.C. 2005. A 3D BEM-FEM methodology for simulation of high speed train induced vibrations. Soil Dynamics and Earthquake Engineering, **25**(4): 289–301. doi:10.1016/j.soildyn.2005.02.005.

Okabe, Z. 1961. Laboratory investigation of railroad ballasts. Bulletin of the Permanent Way Society of Japan, **4**(4): 1–19.

Powrie, W., Yang, L.A., and Clayton, C.R.I. 2007. Stress changes in the ground below ballasted railway track during train passage. Proceedings of the Institution of Mechanical Engineers, Part F: Journal of Rail and Rapid Transit, **221**(2): 247–261. doi:10.1243/0954409JRRT95.

Raymond, G.P. 1978. Design for railroad ballast and subgrade support. Journal of the Geotechnical Engineering Division, ASCE, **104**(1): 45–60.

Raymond, G.P., and Diyaljee, V.A. 1979. Railroad ballast sizing and grading. Journal of the Geotechnical Engineering Division, ASCE, **105**(GT5): 676-681.

Raymond, G.P., and Williams, D.R. 1978. Repeated load triaxial tests on a dolomite ballast. Journal of the Geotechnical Engineering Division, ASCE, **104**(7): 1013–1029.

Sayeed, M.A., and Shahin, M.A. 2015. Modelling of ballasted railway track under train moving loads. *In* Proceedings of the 12th Australia New Zealand Conference on Geomechanics, Wellington, New Zealand. Paper No. 132, pp. 1–8.

Sayeed, M.A., and Shahin, M.A. 2016*a*. Investigation into impact of train speed for behavior of ballasted railway track foundations. Procedia Engineering, **143**: 1152–1159. doi:10.1016/j.proeng.2016.06.131.

Sayeed, M.A., and Shahin, M.A. 2016*b*. Three-dimensional numerical modelling of ballasted railway track foundations for high-speed trains with special reference to critical speed. Transportation Geotechnics, **6**: 55–65. doi:10.1016/j.trgeo.2016.01.003.

Sayeed, M.A., and Shahin, M.A. 2018. Design of ballasted railway track foundations using numerical modelling. Part II: Applications. Canadian Geotechnical Journal, **55**. [This issue.] doi:10.1139/cgj-2016-0634.

Shahin, M.A. 2009. Design of ballasted railway track foundations under cyclic loading. *In* Proceedings of the 2009 GeoHunan International Conference - Slope Stability, Retaining Walls, and Foundations. American Society of Civil Engineers, Changsha, Hunan, China. pp. 68–73.

Shenton, M.J. 1975. Deformation of railway ballast under repeated loading conditions. *In* Proceedings of the Symposium on Railroad Track Mechanics, Princeton University. pp. 387–404.

Stewart, H.E. 1982. The prediction of track performance under dynamic traffic loading. Dissertation, Department of Civil Engineering. University of Massachusetts, Amherst, Mass.

Takemiya, H. 2003. Simulation of track-ground vibrations due to a high-speed train: the case of X-2000 at Ledsgard. Journal of Sound and Vibration, **261**(3): 503–526.

UIC. 1994. Earthworks and trackbed construction for railway lines. UIC Code 719 R. The International Union of Railways, Paris, France.

Yang, L., Powrie, W., and Priest, J.A. 2009. Dynamic stress analysis of a ballasted railway track bed during train passage. Journal of Geotechnical and Geoenvironmental Engineering, **135**(5): 680–689. doi:10.1061/(ASCE)GT.1943-5606.0000032.

List of symbols

A area coefficient
a, b material parameters that depend on subgrade soil type
C_R Raleigh wave velocity
C_s shear wave velocity
c cohesion
E dynamic modulus of elasticity
E_b ballast modulus
E_s subgrade soil modulus
H_b granular layer thickness
H_{bi} thickness of each sublayer of ballast
H_s subgrade layer thickness
H_{si} thickness of each sublayer of subgrade
h thickness of ballast or sub-ballast layer
I moment of inertia
I_ε strain influence factor
I_{ε_b} strain influence factor with depth in ballast layer
I_{ε_s} strain influence factor with depth in subgrade layer
$I_{(\varepsilon\_s)a}$ allowable subgrade surface strain influence factor
I_{ρ_s} subgrade deformation influence factor
$I_{(\rho\_s)a}$ allowable subgrade deformation influence factor
L length coefficient
L_a distance between axles
L_b distance between two bogies
L_c carriage length
l sleeper length
m material parameter that depends on subgrade soil type
N_b number of load applications on ballast layer
N_{bi} number of load cycles in ballast for wheel load P_{si}
N_{bi}^0 equivalent load cycles corresponding to maximum static wheel load, P_s
N_s number of load applications in subgrade layer
N_{si} number of load cycles in subgrade for wheel load P_{si}

N_{si}^{0} equivalent number of load cycles of maximum static wheel load, P_s
P_d design dynamic wheel load
P_F front wheel load
P_R rear wheel load
P_s maximum static wheel load
T_i total traffic tonnage of wheel load, P_{si}
w sleeper width
x, y, z regression parameters that depend on ballast type
α ratio between applied cyclic deviatoric stress andcompressive strength
γ unit weight
ε_{p_b} cumulative plastic strain of ballast
$\varepsilon_{(p\_b)i}$ plastic strain at the centre of each ballast sublayer
ε_{p_s} cumulative plastic strain of track subgrade soil
$\varepsilon_{(p\_s)i}$ plastic strain at the center of each subdivided subgrade layer
$\varepsilon_{(p\_s)a}$ allowable plastic strain at subgrade surface
ν Poisson's ratio
ξ damping ratio
σ_1 major principal stress
σ_3 minor principal stress (confining pressure is a secondary factor)
σ_d deviatoric stress
σ_{d_b} applied cyclic deviatoric stress on ballast
σ_{d_s} deviatoric stress applied to subgrade
$\sigma_{(d\_s)a}$ allowable deviatoric stress at the subgrade surface
σ_{s_b} static strength of ballast under confining pressure of 50 kPa
σ_{s_s} unconfined compressive strength of subgrade soil
ρ_b contribution to track deformation by ballast layers
ρ_s contribution to track deformation by subgrade layer
ρ_t total cumulative plastic deformation of rack under repeated train loading
ρ_{ta} allowable deformation of track for design traffic tonnage
ϕ friction angle (°)